




A Novel Method for the Measurement of Retinal Arteriolar Bifurcation

Guangzheng Dai · Sile Yu · Shenming Hu · Xinze Luan ·
Hairu Yan · Xiaoting Wang · Pengfei Song · Xinying Liu ·
Xingru He 

Received: November 23, 2023 / Accepted: December 21, 2023 / Published online: January 31, 2024
© The Author(s) 2024

ABSTRACT

Introduction: The purpose of this research was to develop protocols for evaluating the bifurcation parameters of retinal arteriole and establish a reference range of normal values.

Methods: In this retrospective study, we measured a total of 1314 retinal arteriolar bifurcations from 100 fundus photographs. We selected 200 from these bifurcations for testing inter-measurer and inter-method agreement. Additionally, we calculated the normal reference range for retinal arteriolar bifurcation parameters and analyzed the effects of gender, age, and anatomical features on retinal arteriolar bifurcation.

Supplementary Information The online version contains supplementary material available at <https://doi.org/10.1007/s40123-023-00881-z>.

S. Yu · S. Hu · X. Luan · X. Wang · X. He (✉)
Department of Public Health, He University,
Shenyang 110034, China
e-mail: hexingru@huh.edu.cn

G. Dai · H. Yan · X. Liu
Dragonfleye Healthcare Technology LLC, Shenyang,
China

G. Dai
He Eye Specialist Hospital, Shenyang, China

P. Song
Dalian Medical University, Dalian, China

Results: The measurement method proposed in this study has demonstrated nearly perfect consistency among different measurers, with inter-class correlation coefficient (ICC) for all bifurcation parameters of retinal arteriole exceeding 0.95. Among healthy individuals, the retinal arteriolar caliber was narrowest in young adults and increased in children, teenagers, and the elderly; retinal arteriolar caliber was greater in females than in males; and the diameter of the inferior temporal branch exceeded that of the superior temporal branch. The angle between the two branches of retinal arteriolar bifurcation was also greater in females than in males. When using the center of the optic disc as a reference point, the angle between the two branches of the retinal arteriole at the proximal or distal ends increased. In contrast, the estimated optimum theoretical values of retinal arteriolar bifurcation were not affected by these factors.

Conclusions: The method for the measurement of retinal arteriolar bifurcation in this study was highly accurate and reproducible. The diameter and branching angle of the retinal arteriolar bifurcation were more susceptible to the influence of gender, age, and anatomical features. In comparison, the estimated optimum theoretical values of retinal arteriolar bifurcation were relatively stable.

Video available for this article.

Keywords: Influencing factors; Measurement method; Retinal arteriole bifurcation

Key Summary Points

Why carry out this study?

In the field of retinal vascular analysis, there has been no standardized measurement for the bifurcation of retinal arterioles. Our study aims to establish a fast, stable, and accurate method for measuring the bifurcation of retinal arterioles.

In healthy individuals, we established the reference range of the retinal arteriolar bifurcation parameters.

We also analyzed the factors that potentially influence the bifurcation of retinal arterioles.

What was learned from the study?

Readers will learn about a standardized measurement process for retinal arteriolar bifurcation, including calculation methods and the measured parameters.

Readers will gain an understanding of the geometric morphological features of retinal arteriolar bifurcations, as well as the factors that influence these features.

higher rates of cardiovascular mortality [2–5]. The assessment of microvascular structure and function has not advanced as rapidly as the noninvasive assessment of larger arteries, primarily due to technical complexities involved in making such measurements. Presently, the primary techniques used to evaluate microcirculation include skin videomicroscopy, skin laser-Doppler flowmetry, flow motion, retinal videomicroscopy, and retinal photography [6].

With the advancement of retinal imaging technology, color fundus photography has provided a secure, cost-effective, and efficient method for capturing images of retinal vessels [7–9]. This approach has enabled researchers to assess the physical characteristics of the retinal vessels without the need for invasive procedures. In recent years, an increasing number of studies have utilized the retinal vasculature as a means to gain insight into the overall health of the cardiovascular system [10, 11]. The primary geometric morphometric parameters of retinal vessels currently utilized include diameter [12–16], fractal dimension [17–20], curvature [21–23], and branching pattern [24, 25].

Of all the parameters, the retinal bifurcation pattern has been the least studied. A small number of studies have attempted to establish the association of retinal arteriolar bifurcation parameters with diabetes [26, 27], hypertension [25], stroke [28], cognitive impairment [29], coronary heart disease [30], and peripheral vascular disease [31]. Unfortunately, some investigations failed to establish any correlation, while others yielded conflicting outcomes. One primary reason for this issue has been the lack of uniform measurement criteria. Firstly, it is important to determine the specific location for vascular bifurcation measurement, including which branch of the central retinal artery/vein to measure and the distance from the optic disc where the measurement should be taken. Secondly, it is crucial to establish the specific range of measurement and ensure that any data falling outside of this range are excluded from the calculation. Lastly, it is important to clearly define the parameters that need to be measured and calculated. According to the established physiological principles of the cardiovascular network proposed by Murray in 1927 [32–34],

DIGITAL FEATURES

This article is published with digital features, including a video, to facilitate understanding of the article. To view digital features for this article, go to <https://doi.org/10.6084/m9.figshare.24885288>.

INTRODUCTION

Cardiovascular diseases have been the leading cause of global mortality for the past 15 years [1]. Microvascular dysfunction has played a significant role in the development and progression of cardiovascular diseases, leading to

maintaining the bifurcation pattern of microcirculation in an optimal state ensures efficient blood transport to terminal organs with minimal energy consumption. Even when factors affect the physiological function of microvasculature, a compensatory mechanism maintains it within the optimal range until compensation is lost. Therefore, accurately obtaining the parameters of microvascular bifurcation is crucial for accessing the cardiovascular system. The main objective of this research was to develop a standardized protocol for assessing the retinal arteriolar bifurcation and establish a reference range of normal values.

METHODS

Study Design

This was a single-center, retrospective, randomized, single-blind study conducted in accordance with the Declaration of Helsinki. The protocol received approval from the Institutional Review Board (IRB2019.K010.01) of He Eye Specialist Hospital. All participants were recruited from the Health Examination Center at He Eye Specialist Hospital. Following the application of the exclusion criteria detailed in Table 1, we enrolled 100 subjects, comprising 54 males and 46 females, with ages ranging from 3 to 80 years and a mean age of 39.6 ± 22.2 years. All subjects or their legal guardians gave written informed consent, and minors gave assent.

Ophthalmological Examination

All subjects underwent a comprehensive standard ophthalmological examination. Visual acuity was assessed using the Standard Logarithmic Visual Acuity Chart. Refractive errors were determined using an autokerato-refractometer (KR-8100, Topcon, Tokyo, Japan). Intraocular pressure was measured with a non-contact tonometer (CT-800, Topcon, Tokyo, Japan). Slit-lamp microscopy (LS-5, Sunkingdom Medical Instrument, Chongqing, China) was utilized to examine the anterior segment and fundus.

Table 1 Exclusion criteria

1	Patients with moderate/high myopia
2	Patients with moderate/high hyperopia
3	Patients with moderate/high astigmatism
4	Patients with refractive media opacity (e.g., cataracts, fundus hemorrhage, and similar conditions, which may hinder clear fundus photography)
5	Patients with small pupils, making it difficult to capture complete photographs of the back of the eye (e.g., in the case of glaucoma)
6	Patients with ocular diseases leading to abnormalities in the retinal blood vessels (e.g., central retinal arterial or venous obstruction, and ischemic optic neuropathy)
7	Patients with fundus photographs that do not meet the specified criteria (e.g., underexposure, criteria, such as underexposure, overexposure, missing anatomical structures such as the optic disc or macula, and artifacts)
8	Patients with diabetes mellitus
9	Patients with hypertension
10	Patients with hyperlipidemia
11	Patients with obesity
12	Patients with a history of cardiovascular and cerebrovascular diseases

Assessment of Cardiovascular Risk Factors

All participants were interviewed and assessed for cardiovascular risk factors. Resting blood pressure was evaluated following a standardized protocol, and hypertension was defined by having self-reported antihypertensive medication use, systolic blood pressure ≥ 140 mmHg, or diastolic blood pressure ≥ 90 mmHg. Body mass index (BMI) was calculated as weight in kilograms divided by the square of height in

meters. Fasting venous blood samples were collected from participants after an 8-h fast to measure serum glucose, lipids, and lipoproteins. Diabetes mellitus was defined as fasting plasma glucose ≥ 7.0 mmol/l, 2-h post-load glucose levels ≥ 11.1 mmol/l, or use of diabetes medication (insulin or oral). Additionally, detailed clinical records, including age, sex, occupation, smoking status, alcohol consumption, and family and cardiovascular disease history, were collected for each participant.

Retinal Photography and Retinal Image Preprocessing

Color fundus photographs, centered on the macula, were obtained from a single eye of each participant by trained technicians using a 45° non-mydratic digital camera (TRC-NW300, Topcon, Tokyo, Japan). For each participant, generate a random number between 1 and 2, where 1 represents the left eye and 2 represents the right eye. Each fundus photograph was compressed into JPG format and saved as a JPG file. We stored the photographs in three separate color channels (red, green, blue) to preserve complete color information. Each individual fundus photograph had dimensions of 2048 × 1536 pixels and a resolution of 96 dots per inch (dpi). The photographs were cropped to the field of view (FOV) and resized to 2048 × 2048 pixels, as shown in Fig. 1a. After cropping the images, the ratio of the vertical diameter to the

horizontal diameter of FOV remained unchanged.

Automatic Measurement Method of Retinal Arteriolar Bifurcation

The process involved several steps, including the segmentation of retinal vessels, selection of the bifurcation area, extraction of the bifurcation skeleton, calculation of the center point coordinates, identification of the effective measurement area, and measurement of the diameter and branch angle. Semantic segmentation of retinal vessels in fundus images was performed using the SeqNet segmentation network [35], resulting in the segmented images shown in Fig. 1b. Notably, the method improved the AUC to 0.98 for segmentation and achieved an accuracy of 0.92 over the DRIVE dataset.

To measure the retinal arteriolar bifurcation, a 321 × 321 px subgraph was created with a field of view radius of 110 px, as shown in Fig. 1c. The generated subgraph was used to extract skeleton lines for the selected retinal arteriolar bifurcations, from which the coordinates of the intersection points of the three skeleton lines were calculated, shown in Fig. 1d.

Two green concentric circles were utilized to define the measurement area. The smaller circle had a radius of 15 px, while the larger circle had a radius of 65 px, delineating the 50-px-wide annular region representing the valid measurement area of the retinal arteriolar bifurcation, as

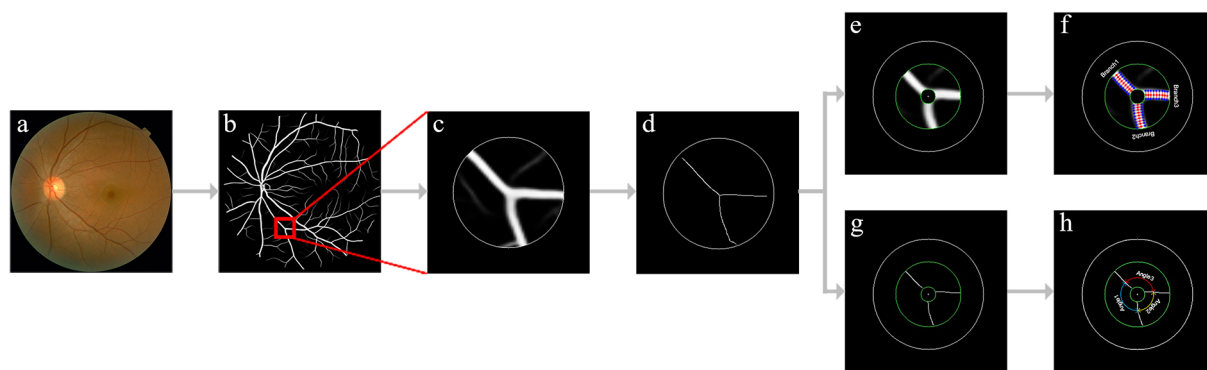


Fig. 1 Process for calculating retinal arteriole bifurcation parameters

depicted in Fig. 1e and g. For each pixel point on the skeleton line within the valid measurement area of the retinal arteriolar bifurcation, a diameter line perpendicular to the skeleton line was drawn. The width of the retinal arteriole was calculated at each pixel point along the skeleton line, and the average value was regarded as the overall width. The unit of measurement is expressed in pixels, as shown in Fig. 1f. Originating from the parent vessel and rotating counterclockwise, these branches are referred to as Branch1, Branch2, and Branch3.

Furthermore, a circle centered at the bifurcation point with a radius of 40 px was depicted, as illustrated in Fig. 1h. The circle intersects with three radial skeletal lines, creating three angles. Originating from the parent vessel and rotating counterclockwise, these angles are referred to as Angle1, Angle2, and Angle3.

Calculation of Retinal Arteriolar Bifurcation Parameters

To depict the bifurcation pattern of the retinal arteriole more accurately, we converted the direct measurements (Branch1, Branch2, Branch3, Angle1, Angle2, and Angle3). A retinal arteriolar bifurcation is defined by the diameters d_0 , d_1 , and d_2 of the parent vessel, the larger branch, and the smaller branch, respectively, as well as the angles θ_1 and θ_2 . These angles represent the orientation of the larger and smaller branches in relation to the direction of the parent vessel, as illustrated in Fig. 2. The total angle θ is the sum of θ_1 and θ_2 .

The “asymmetry ratio”, represented by the symbol α , is the ratio of the cross-sectional area

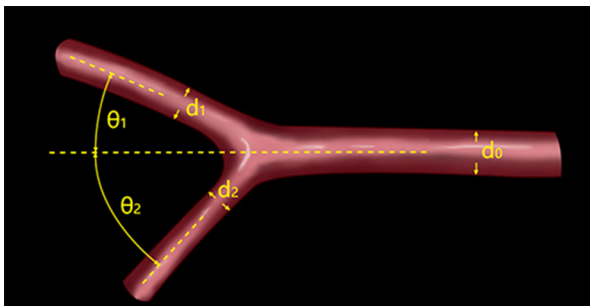


Fig. 2 Schematic diagram of retinal arteriolar bifurcation

of the smaller branch to that of the larger branch.

$$\alpha = d_2^2/d_1^2$$

The sum of the cross-sectional areas of the two branches divided by that of the parent artery is generally referred to as

The “area ratio”, denoted by the symbol β , is typically defined as the total cross-sectional area of the two branches divided by that of the parent artery.

$$\beta = (d_1^2 + d_2^2)/d_0^2.$$

Retinal vascular geometric morphological parameters have been shaped by the physiological principles of the cardiovascular network, as originally proposed by Murray in 1927 [34]. Subsequently, Murray’s principles have evolved to encompass four main tenets: minimum lumen volume, minimum lumen surface, minimum pumping power, and minimum drag [36, 37].

The angles θ_1^{vp} and θ_2^{vp} represent the estimated optimal theoretical values based on minimum lumen volume and pumping power considerations.

$$\cos\theta_1^{vp} = \left[(1 + \alpha^{3/2})^{4/3} + 1 - \alpha^2 \right] / 2(1 + \alpha^{3/2})^{2/3}$$

$$\cos\theta_2^{vp} = \left[(1 + \alpha^{3/2})^{4/3} + \alpha^2 - 1 \right] / 2\alpha(1 + \alpha^{3/2})^{2/3}$$

The angles θ_1^{sd} and θ_2^{sd} represent the estimated optimal theoretical values based on the minimum lumen surface and drag considerations.

$$\cos\theta_1^{sd} = \left[(1 + \alpha^{3/2})^{2/3} + 1 - \alpha \right] / 2(1 + \alpha^{3/2})^{1/3}$$

$$\cos\theta_2^{sd} = \left[(1 + \alpha^{3/2})^{2/3} + \alpha - 1 \right] / 2\alpha^{1/2}(1 + \alpha^{3/2})^{1/3}$$

The average of the two optimal predictions is considered as the theoretical optimum value of the angle, denoted as θ_1' and θ_2' respectively.

$$\theta_{1'} = (\theta_1^{vp} + \theta_1^{sd})/2$$

$$\theta_{2'} = (\theta_2^{vp} + \theta_2^{sd})/2$$

Manual Measurement Method of Retinal Arteriolar Bifurcation

In contrast to the automated measurement method proposed in this study, we developed a manual measurement scheme for assessing the bifurcation parameters of retinal arteriole using ImageJ software. The manual process involved the following steps: manually selecting the center point of the retinal arteriolar bifurcation, measuring the angles between the two branches and the parent vessel with the central point as the vertex (Angle1 and Angle3), calculating the angle between the two branches by subtracting the sum of these angles from 360 degrees (Angle2), and measuring the width of the three branches at a distance of 40 pixels from the center point (Branch1, Branch2, and Branch3). We selected 200 retinal arteriolar bifurcations from 100 retinal photographs (consisting of one superior temporal and one inferior temporal branch from each photograph). Three trained ophthalmologists applied both methods to measure these bifurcations, and a consistency analysis was conducted on the measurement results.

Statistical Analysis

We conducted statistical analysis using the Statistical Package for the Social Sciences (SPSS, version 27.0). Statistical significance was defined as a p value < 0.05 . Continuous variables were expressed as mean \pm SD, and categorical variables as percentages. The independent Student t test was used to compare continuous variables between two groups, and univariate analysis of variance (UANOVA) was used for comparisons among three groups. Pairwise comparisons among multiple groups were performed using a post hoc analysis with Bonferroni correction. To assess the main effects of retinal arteriole bifurcation parameters, we used multivariate analysis of variance (MANOVA).

We also calculated the interclass correlation coefficient (ICC) to describe inter-measurer (using two-way random-effects model, absolute agreement, single measurement) and inter-method (using two-way mixed-effects model, consistency, single measurement) agreement for the bifurcation parameters of the retinal arteriole.

RESULTS

We compared the manual measurement of retinal arteriolar bifurcations with the automated method proposed in this study. The results of these measurements are shown in Tables 2 and 3, with Branch1 representing the parent vessel and subsequent branches labeled as Branch2 and Branch3, forming angles Angle1, Angle2, and Angle3. A, B, and C denote the three different individuals who conducted the measurements. Our findings demonstrated that the method proposed in this study for the measurement of retinal arteriolar bifurcation exhibited greater repeatability compared to traditional manual measurement methods. Furthermore, we compared the time required to measure retinal arteriolar bifurcation using two techniques. The automated measurement method takes approximately 15 s to complete the measurement and recording of a retinal arteriolar bifurcation, while the manual measurement method takes around 30 s.

In this study, we analyzed nearly all the retinal arterial bifurcations present in 100 retinal fundus images, amounting to a total of 1314. The parameters of the retinal arteriolar bifurcation were analyzed separately for age, gender, and anatomical features, and the results are summarized in Table 4. The participants were categorized into four age groups (0–20 years, 20–40 years, 40–60 years, and 60–80 years) based on biological and physiological similarities within each age group. The impact of age on retinal arterioles was mainly reflected in a smaller retinal arteriolar caliber among young adults. The results showed that men had a smaller retinal arteriolar caliber and branching angle θ compared to women. The results

Table 2 Inter-measurer agreements of retinal arteriole bifurcations

Method	Parameter	Measurer	Mean ± SD	ICC	P_1	F	P_2
Automatic-measurement	Angle1 (degree)	A	139.18 ± 14.81				
		B	139.20 ± 14.83	0.99	< 0.001	0.01	0.986
		C	139.41 ± 14.76				
	Angle2 (degree)	A	85.23 ± 14.58				
		B	85.16 ± 14.79	0.99	< 0.001	0.01	0.994
		C	85.07 ± 14.63				
	Angle3 (degree)	A	135.59 ± 14.28				
		B	135.63 ± 14.55	0.99	< 0.001	0.00	0.997
		C	135.52 ± 14.51				
	Branch1 (px)	A	21.86 ± 3.32				
		B	21.76 ± 3.29	0.95	< 0.001	0.71	0.492
		C	21.48 ± 3.27				
	Branch2 (px)	A	20.22 ± 3.45				
		B	20.15 ± 3.47	0.96	< 0.001	0.86	0.422
		C	19.80 ± 3.44				
Branch3 (px)	A	20.26 ± 3.70					
	B	20.15 ± 3.73	0.97	< 0.001	0.76	0.470	
	C	19.82 ± 3.68					
Manual measurement	Angle1 (degree)	A	141.13 ± 18.19				
		B	140.38 ± 15.60	0.90	< 0.001	0.19	0.830
		C	141.37 ± 16.96				
	Angle2 (degree)	A	81.05 ± 13.52				
		B	81.31 ± 12.96	0.85	< 0.001	0.82	0.442
		C	79.76 ± 12.47				
	Angle3 (degree)	A	137.82 ± 16.93				
		B	137.56 ± 18.61	0.92	< 0.001	0.43	0.648
		C	139.11 ± 17.88				
Branch1 (px)	A	12.10 ± 2.64					
	B	10.67 ± 2.48	0.45	< 0.001	29.19	< 0.001	
	C	12.58 ± 2.66					

Table 2 continued

Method	Parameter	Measurer	Mean \pm SD	ICC	P_1	F	P_2
	Branch2 (px)	A	10.14 \pm 2.39	0.26	< 0.001	64.33	< 0.001
		B	8.38 \pm 1.88				
		C	10.70 \pm 2.10				
	Branch3 (px)	A	10.23 \pm 2.45	0.47	< 0.001	53.22	< 0.001
		B	8.54 \pm 2.14				
		C	10.91 \pm 2.49				

Automatic measurement the method for the measurement of retinal arteriolar bifurcation proposed in this study; *Manual measurement* the measurement of retinal arteriolar bifurcation using the ImageJ software; *A, B, C* the three different measurer; *ICC* interclass correlation coefficient; P_1 statistical significance based on ICC; F statistic in standard univariate analysis of variance; P_2 statistical significance based on univariate analysis of variance; *SD* standard deviation

indicated no significant disparity in data between the right and left eyes. The distance from the optic disc, the branches to which the arterial bifurcation belongs, asymmetry ratio, and area ratio of the retinal arteriolar bifurcation were all thought to be important influencing factors for bifurcation parameters of retinal arteriole. The measurements for distance, asymmetry ratio, and area ratio were sorted in ascending order and then grouped into three equal parts according to quartiles. The results indicated that these anatomical features had a more pronounced influence on the characteristics of retinal arteriolar branching on the retinal arteriolar bifurcation.

Table 5 presents the results of the multivariate analysis of variance and parameter estimates for each aspect of the retinal arteriolar bifurcation. The parameter estimates illustrate the differences in estimated marginal means compared to the reference level, denoted as “Ref” in the table. NA indicated that this variable had no statistical correlation with the dependent variable after controlling for other confounding factors and was not included in the final model. The analysis revealed that nearly all the factors under investigation had a profoundly significant impact on retinal arteriolar caliber. Among healthy individuals, the retinal arteriolar caliber was narrowest in young adults and increased in children, teenagers, and the elderly; retinal arteriolar caliber was greater

in females than in males; and the diameter of the inferior temporal branch exceeded that of the superior temporal branch. Factors influencing retinal arteriolar branching angle were relatively few. The angle between the two branches of retinal arteriolar bifurcation was larger in females than in males. When using the center of the optic disc as a reference point, the angle between the two branches of the retinal arteriole at the proximal or distal ends increased. Age, gender, the distance from the optic disc and the branches to which the arterial bifurcation belongs had no effect on the estimated optimum theoretical values of retinal arteriolar bifurcation.

DISCUSSION

The retinal vasculature serves as a “window” into the entire cardiovascular system, providing significant scientific and practical value [38, 39]. Therefore, it was crucial to develop a fast, accurate, and reproducible method for the quantitative assessment of retinal vessels. In this study, the method for measuring retinal arteriolar bifurcation showed high repeatability across different measurers. Compared with traditional manual measurement methods, it provided stable measurements of retinal arteriolar caliber. The retinal arteriole appeared significantly thinner in fundus photographs, leading

Table 3 Inter-method agreements of retinal arteriole bifurcations

Measurer	Parameter	Method	Mean \pm SD	ICC	P_1	F	P_2
A	Angle1 (degrees)	Automatic	139.18 \pm 14.81	0.85	< 0.001	1.38	0.241
		Manual	141.13 \pm 18.19				
	Angle2 (degrees)	Automatic	85.23 \pm 14.58	0.89	< 0.001	8.82	0.003
		Manual	81.05 \pm 13.52				
	Angle3 (degrees)	Automatic	135.59 \pm 14.28	0.83	< 0.001	2.03	0.155
		Manual	137.82 \pm 16.93				
	Branch1 (px)	Automatic	21.86 \pm 3.32	0.45	< 0.001	1058.66	< 0.001
		Manual	12.10 \pm 2.64				
	Branch2 (px)	Automatic	20.22 \pm 3.45	0.40	< 0.001	1151.31	< 0.001
		Manual	10.14 \pm 2.39				
	Branch3 (px)	Automatic	20.26 \pm 3.70	0.34	< 0.001	1020.80	< 0.001
		Manual	10.23 \pm 2.45				
B	Angle1 (degrees)	Automatic	139.20 \pm 14.83	0.89	< 0.001	0.60	0.440
		Manual	140.38 \pm 15.60				
	Angle2 (degrees)	Automatic	85.16 \pm 14.79	0.88	< 0.001	7.67	0.006
		Manual	81.31 \pm 12.96				
	Angle3 (degrees)	Automatic	135.63 \pm 14.55	0.78	< 0.001	1.33	0.250
		Manual	137.56 \pm 18.61				
	Branch1 (px)	Automatic	21.76 \pm 3.29	0.24	< 0.001	1448.73	< 0.001
		Manual	10.67 \pm 2.48				
	Branch2 (px)	Automatic	20.15 \pm 3.47	0.08	0.127	1777.93	< 0.001
		Manual	8.38 \pm 1.88				
	Branch3 (px)	Automatic	20.15 \pm 3.73	0.14	0.027	1458.55	< 0.001
		Manual	8.54 \pm 2.14				

Table 3 continued

Measurer	Parameter	Method	Mean \pm SD	ICC	P_1	F	P_2
C	Angle1 (degrees)	Automatic	139.41 \pm 14.76	0.87	< 0.001	1.52	0.218
		Manual	141.37 \pm 16.96				
	Angle2 (degrees)	Automatic	85.07 \pm 14.63	0.87	< 0.001	15.27	< 0.001
		Manual	79.76 \pm 12.47				
	Angle3 (degrees)	Automatic	135.52 \pm 14.51	0.78	< 0.001	4.87	0.028
		Manual	139.11 \pm 17.88				
	Branch1 (px)	Automatic	21.48 \pm 3.27	0.28	< 0.001	892.57	< 0.001
		Manual	12.58 \pm 2.66				
	Branch2 (px)	Automatic	19.80 \pm 3.44	0.18	0.006	1020.00	< 0.001
		Manual	10.70 \pm 2.10				
	Branch3 (px)	Automatic	19.82 \pm 3.68	0.35	< 0.001	806.54	< 0.001
		Manual	10.91 \pm 2.49				

A, B, C the three different measurer; *Automatic* the method for the measurement of retinal arteriolar bifurcation proposed in this study; *Manual* the measurement of retinal arteriolar bifurcation using ImageJ software; *ICC* interclass correlation coefficient; P_1 statistical significance based on ICC; F statistic in standard univariate analysis of variance; P_2 statistical significance based on univariate analysis of variance; *SD* standard deviation

to unavoidable subjective errors in manual measurements when a measurer lacked sufficient training. The research findings indicated that the retinal arteriolar diameter obtained using the method proposed in this study are significantly larger than those obtained through manual measurements. We conducted an analysis for these results and believe that the following reasons are primarily responsible. Since the wall of the retinal arteriole was transparent, the visible feature in the retinal image was the blood column itself. Therefore, the diameter we measured on the retinal fundus image was actually the width of the blood column, which was narrower than the actual blood vessel width. Upon careful observation, it can be noticed that there was a fuzzy band around the retinal arteriole. Our measurement method accounted for this fuzzy band as part of the arteriolar diameter, as indicated by the black dotted line in Fig. 3b, whereas manual

measurements typically exclude this portion, as shown by the blue dotted line in Fig. 3b.

In addition to traditional manual measurement methods, some studies have introduced semi-automated computer-assisted measurements of retinal arteriolar bifurcation parameters. The most extensively utilized application was the Singapore I Vessel Assessment (SIVA) created by the Department of Computer Science at the National University of Singapore [24–28, 30, 40–42]. Some studies also utilized a custom-written application package within the MATLAB environment to measure retinal arteriolar bifurcation parameters [29, 31]. Compared with these measurement methods, the approach proposed in this study was more comprehensive, specifically manifested as follows: (1) Introducing a deep learning algorithm for the segmentation of retinal vessels, further enhancing the accuracy of measuring retinal arteriolar bifurcation parameters; (2) Dividing the bifurcation angle theta into θ_1 and θ_2 for

Table 4 Univariate analysis of retinal arteriole bifurcations

Factor	Level(num)	d_0 (px)	d_1 (px)	d_2 (px)	θ_1 (degree)	θ_2 (degree)	θ (degree)	$\theta_1/(\text{degree})$	$\theta_2/(\text{degree})$	$\theta/(\text{degree})$
Age	0–20 (347)	19.01 ± 4.55	18.64 ± 4.69	14.96 ± 4.12	32.92 ± 17.13	49.39 ± 17.84	82.30 ± 14.91	35.76 ± 6.53	52.70 ± 6.60	88.46 ± 0.08
	20–40 (365)	17.57 ± 4.07	17.17 ± 4.38	13.58 ± 4.36	29.95 ± 16.23	52.21 ± 17.78	82.16 ± 14.34	35.00 ± 7.60	53.47 ± 7.70	88.47 ± 0.09
	40–60 (320)	18.24 ± 4.22	17.81 ± 4.32	13.89 ± 4.51	30.36 ± 16.14	50.38 ± 17.38	80.74 ± 13.89	34.29 ± 7.46	54.19 ± 7.54	88.47 ± 0.09
	60–80 (282)	18.39 ± 3.90	18.20 ± 4.15	13.74 ± 4.68	29.96 ± 16.40	53.26 ± 18.31	83.22 ± 15.24	33.01 ± 8.70	55.49 ± 8.81	88.50 ± 0.12
Gender	Female (603) (702)	$P < 0.001$	$P < 0.001$	$P < 0.001$	$P = 0.055$	$P = 0.027$	$P = 0.214$	$P < 0.001$	$P < 0.001$	$P < 0.001$
	Male (711)	18.59 ± 4.29	18.24 ± 4.46	14.28 ± 4.28	31.00 ± 16.30	52.17 ± 16.92	83.16 ± 14.23	34.66 ± 7.11	53.82 ± 7.18	88.47 ± 0.08
Eye	OD (748)	18.04 ± 4.18	17.68 ± 4.40	13.86 ± 4.56	30.70 ± 16.72	50.46 ± 18.59	81.16 ± 14.84	34.56 ± 8.02	53.92 ± 8.12	88.48 ± 0.10
	OS (566)	$P = 0.013$	$P = 0.016$	$P = 0.073$	$P = 0.753$	$P = 0.065$	$P = 0.009$	$P = 0.816$	$P = 0.803$	$P = 0.105$
Branch	OD (748)	18.41 ± 4.25	18.00 ± 4.56	14.19 ± 4.48	31.11 ± 16.02	50.61 ± 17.78	81.72 ± 14.97	34.86 ± 7.38	53.62 ± 7.46	88.47 ± 0.09
	OS (566)	18.13 ± 4.21	17.85 ± 4.27	13.87 ± 4.38	30.47 ± 17.16	52.08 ± 17.94	82.55 ± 14.08	34.26 ± 7.90	54.22 ± 7.99	88.48 ± 0.10
Branch	STB (653)	$P = 0.185$	$P = 0.442$	$P = 0.156$	$P = 0.497$	$P = 0.173$	$P = 0.371$	$P = 0.162$	$P = 0.161$	$P = 0.101$
	ITB (661)	18.01 ± 4.25	17.63 ± 4.33	13.75 ± 4.32	31.05 ± 16.62	50.63 ± 18.02	81.68 ± 14.52	34.40 ± 7.54	54.07 ± 7.62	88.48 ± 0.09
Alpha	≤ 0.53 (438)	18.57 ± 4.20	18.23 ± 4.52	14.35 ± 4.54	30.63 ± 16.43	51.85 ± 17.69	82.47 ± 14.66	34.80 ± 7.69	53.68 ± 7.78	88.48 ± 0.10
	≤ 0.78 (438)	$P = 0.017$	$P = 0.015$	$P = 0.014$	$P = 0.646$	$P = 0.219$	$P = 0.326$	$P = 0.350$	$P = 0.354$	$P = 0.854$
Beta	≤ 1.41 (438)	18.24 ± 4.08	18.30 ± 4.30	10.94 ± 3.34	22.42 ± 11.68	58.27 ± 17.28	80.69 ± 14.56	25.67 ± 5.55	62.90 ± 5.66	88.56 ± 0.12
	≤ 1.71 (438)	18.47 ± 4.43	18.11 ± 4.61	14.74 ± 3.84	31.67 ± 16.03	50.60 ± 16.87	82.27 ± 14.58	36.13 ± 2.03	52.31 ± 2.04	88.42 ± 0.01
Distance	≤ 1.00 (438)	18.16 ± 4.18	17.42 ± 4.35	16.48 ± 4.14	38.42 ± 17.24	44.86 ± 16.86	83.27 ± 14.56	42.01 ± 1.40	46.41 ± 1.40	88.44 ± 0.00
	≤ 1.41 (438)	$P = 0.520$	$P = 0.011$	$P < 0.001$	$P < 0.001$	$P < 0.001$	$P = 0.030$	$P < 0.001$	$P < 0.001$	$P < 0.001$
Distance	≤ 1.71 (438)	18.22 ± 4.31	16.58 ± 4.18	11.13 ± 3.54	25.53 ± 14.17	53.27 ± 17.88	78.80 ± 14.87	29.65 ± 5.55	58.88 ± 8.61	88.53 ± 0.13
	≤ 1.666 (438)	18.43 ± 4.29	18.01 ± 4.25	14.24 ± 3.73	28.87 ± 14.48	52.80 ± 17.27	81.66 ± 13.50	35.15 ± 5.79	53.31 ± 5.84	88.46 ± 0.06
Distance	≤ 1.666 (438)	18.20 ± 4.10	19.21 ± 4.49	16.80 ± 4.07	38.11 ± 18.00	47.66 ± 17.92	85.78 ± 14.56	39.00 ± 4.93	49.43 ± 4.97	88.44 ± 0.06
	≤ 1.666 (438)	$P = 0.647$	$P < 0.001$	$P < 0.001$	$P < 0.001$	$P < 0.001$	$P < 0.001$	$P < 0.001$	$P < 0.001$	$P < 0.001$
Distance	≤ 839 (438)	20.88 ± 4.28	20.42 ± 4.69	15.95 ± 4.97	31.95 ± 16.32	50.76 ± 18.02	82.71 ± 16.69	34.36 ± 7.70	54.11 ± 7.78	88.48 ± 0.10
	≤ 1127 (438)	17.61 ± 3.79	17.24 ± 3.96	13.57 ± 4.01	30.90 ± 16.81	49.39 ± 17.94	80.29 ± 14.26	34.82 ± 7.60	53.65 ± 7.68	88.47 ± 0.09
Distance	≤ 1666 (438)	16.39 ± 3.22	16.14 ± 3.39	12.64 ± 3.54	29.66 ± 16.37	53.57 ± 17.39	83.24 ± 12.37	34.62 ± 7.56	53.85 ± 7.63	88.48 ± 0.09
	≤ 1666 (438)	$P < 0.001$	$P < 0.001$	$P < 0.001$	$P = 0.123$	$P = 0.002$	$P = 0.006$	$P = 0.668$	$P = 0.669$	$P = 0.780$

d_0 parent vessel; d_1 the larger branch; d_2 the smaller branch; θ_1 the larger branch make with the direction of the parent vessel; θ_2 the smaller branch make with the direction of the parent vessel; θ the sum of θ_1 and θ_2 ; $\theta_1/\text{optimal}$ prediction for the θ_1 ; $\theta_2/\text{optimal}$ prediction for the θ_2 ; $\theta/\text{optimal}$ prediction for the θ ; θ_1/OD the left eye, θ_2/OS the right eye, θ/Alpha asymmetry ratio, θ_2/Beta area ratio, θ_1/STB superior temporal branch, θ_2/ITB inferior temporal branch

Table 5 Multivariate analysis of retinal arteriole bifurcations

Factor	Level (num)	d_0 (px)	d_1 (px)	d_2 (px)	θ_1 (degree)	θ_2 (degree)	θ (degree)	$\theta_1/(\text{degree})$	$\theta_2/(\text{degree})$	$\theta/(\text{degree})$
Age	0–20 (347)	1.33*	1.27*	1.10*	NA	NA	NA	NA	NA	NA
	20–40 (365)	Ref	Ref	Ref						
	40–60 (320)	0.17	0.07	0.14						
	60–80 (282)	0.52	0.61*	0.48						
Sex	Female (603) (702)	0.62*	0.54*	0.37*	NA	NA	1.85*	NA	NA	NA
	Male (711)	Ref	Ref	Ref			Ref			
Alpha	≤ 0.53 (438)		1.31*	– 2.61*	– 7.75*	8.23*		– 9.75*	9.86*	0.11*
	≤ 0.78 (438)	NA	Ref	Ref	Ref	Ref	NA	Ref	Ref	Ref
	≤ 1.00 (438)		– 1.35*	1.13*	5.20*	– 5.46*		5.67*	– 5.69*	– 0.02*
Beta	≤ 1.41 (438)		– 2.03*	– 2.19*	– 0.28	– 2.83*	– 2.85*	– 1.74*	1.78*	0.03*
	≤ 1.71 (438)	NA	Ref	Ref	Ref	Ref	Ref	Ref	Ref	Ref
	≤ 4.19 (438)		1.93*	1.78*	6.20*	– 2.05	4.13*	0.29	– 0.28	0.01
Branch	STB (653)	– 1.00*	– 1.02*	– 0.79*	NA	NA	NA	NA	NA	NA
	ITB (661)	Ref	Ref	Ref						

Table 5 continued

Factor	Level (num)	d_0 (px)	d_1 (px)	d_2 (px)	θ_1 (degree)	θ_2 (degree)	θ (degree)	$\theta_{1'}$ (degree)	$\theta_{2'}$ (degree)	θ' (degree)
Distance	≤ 839 (438)	3.39*	3.37*	2.76*		0.99	2.63*			
	≤ 1127 (438)	Ref	Ref	Ref	NA	Ref	Ref	NA	NA	NA
	≤ 1666 (438)	–	–	–		4.00*	2.77*			

d_0 parent vessel, d_1 the larger branch, d_2 the smaller branch, θ_1 the larger branch make with the direction of the parent vessel, θ_2 the smaller branch make with the direction of the parent vessel, θ the sum of θ_1 and θ_2 , $\theta_{1'}$ optimal prediction for the θ_1 ; $\theta_{2'}$ optimal prediction for the θ_2 ; θ' the sum of $\theta_{1'}$ and $\theta_{2'}$, *OS* the left eye, *OD* the right eye, *Alpha* asymmetry ratio, *Beta* area ratio, *STB* superior temporal branch, *ITB* inferior temporal branch, *NA* while constructing the MANOVA model, this particular factor was not incorporated into the model, *Ref* this parameter is set to zero because it is redundant
 * p value less than 0.05

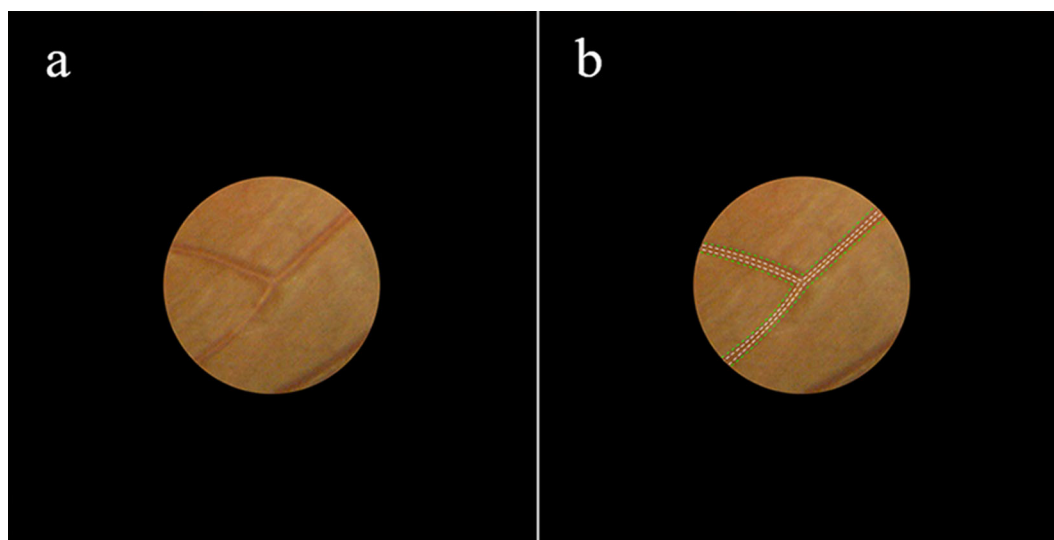


Fig. 3 Comparison of manual measurement and automatic measurement of retinal arteriolar diameter

measurement and analysis; (3) Measuring not only the bifurcation angle at the bifurcation but also the width of the branch arteries; (4) Not only measuring the actual bifurcation angle but also calculating the optimal theoretical value; (5) Detailed recording of the arterial branches to which the bifurcation belongs, the distance from the optic disc.

However, the method for the measurement of retinal arteriolar bifurcation proposed in this

paper also had some limitations. First, this method was not fully automated measurement, as it required a mouse to click and select the retinal arteriolar bifurcation to be measured. The position of the mouse click will minimally impact the final measurement result. Second, measuring certain retinal arteriolar bifurcations can be challenging, particularly those with short trunks (as shown in Fig. 4a and b), or where a retinal venule travels within arteriolar

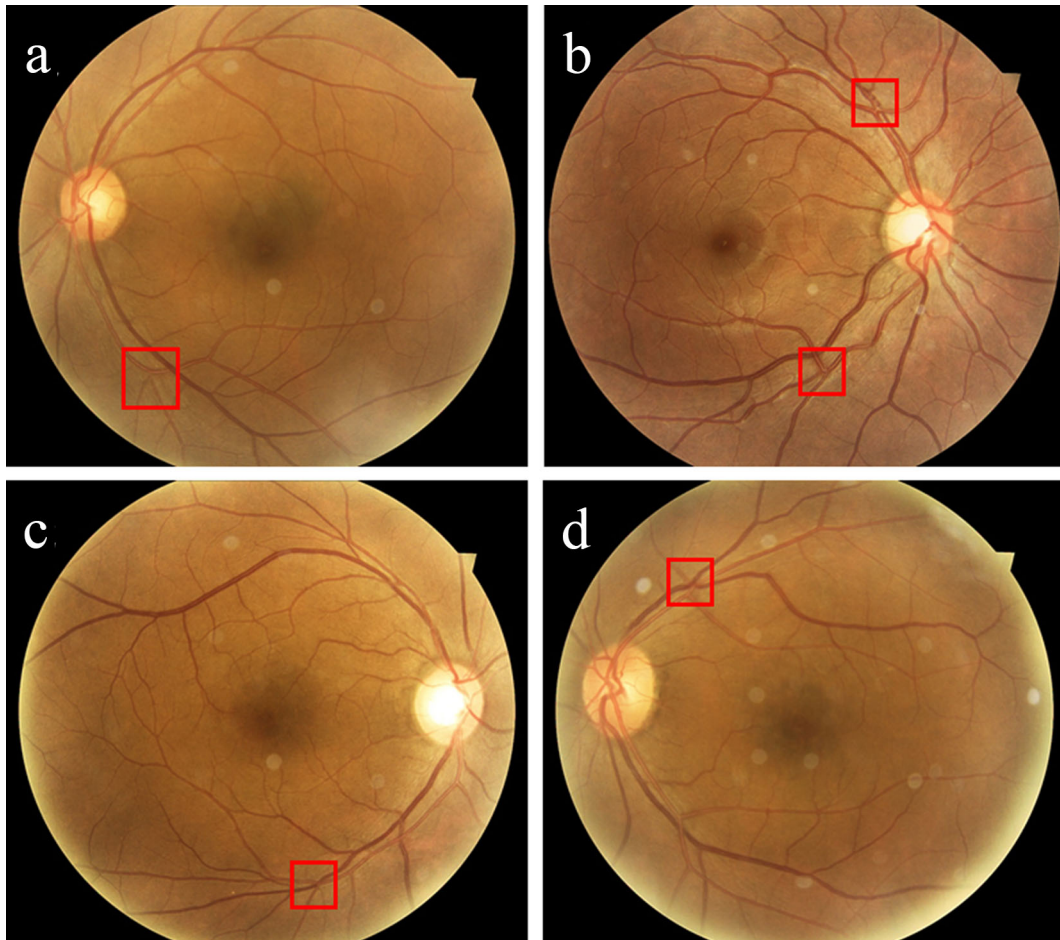


Fig. 4 Examples of retinal arteriole bifurcation that cannot be measured

bifurcations (as depicted in Fig. 4c and d). Third, the measuring method proposed in this study, by cropping the fundus photos, retained only the effective field of view and uniformly scaled them to 2048×2048 . This step aimed to ensure the comparability of absolute parameters, such as retinal arteriole diameter, among fundus photos of different sizes. However, the varying imaging parameters of different fundus cameras made this comparability unreliable, and this study had not yet identified alternative relative parameters.

This study analyzed the retinal arteriolar bifurcation pattern in fundus images from 100 healthy individuals and established a normal reference range. Age, gender, asymmetry ratio, area ratio, the distance from the optic disc, and the branches to which the arterial bifurcation

belongs were all significant factors in determining retinal arteriolar caliber. The result was consistent with some previous research results [43, 44]. There were relatively few factors that influenced the branching angle of retinal arterioles. The most stable estimated optimum theoretical values were primarily influenced by the asymmetry ratio and area ratio. However, these two factors were artificially determined based on the ratio relationship between three blood branches, making their impact on the optimal theoretical value unavoidable. Despite the potential effects of age, gender, and anatomical features on the diameter of the retinal arteriole, the estimated optimum theoretical values remained unaffected and stable. The calculation of the optimal theoretical value relied on the asymmetry ratio, which tended to

remain stable even when the retinal arteriolar diameter fluctuated. Essentially, when the retinal arteriolar bifurcations were not significantly influenced by obvious pathophysiological factors, the estimated optimum theoretical values would remain at a stable level. The author suggested that the factors responsible for these parameter changes could have a significant impact on pathological and physiological changes in the cardiovascular system.

In the upcoming research, we will use this tool to extract a large number of retinal arteriolar bifurcation parameters from a high-risk cardiovascular disease population and analyze their correlation with cardiovascular risk factors. Our aim is to further explore the feasibility of utilizing retinal vessels as an early warning signal for cardiovascular disease.

CONCLUSIONS

In this paper, we present a fast, stable, and accurate method for measuring retinal arteriolar bifurcations and establishing a reference range of normal values. The diameter and branching angle of the retinal arteriolar bifurcations were significantly influenced by gender, age, and anatomical features, while the estimated optimal theoretical values of retinal arteriolar bifurcations remained relatively stable.

ACKNOWLEDGEMENTS

We thank the participants in this study. This work was supported by Dragonfleye Healthcare Technology LLC and He Eye Specialist Hospital, Shenyang, China. The authors have no proprietary interest in any of the products mentioned in this article.

Author Contributions. Conceptualization: Xingru He, Guangzheng Dai, Sile Yu, Shenming Hu; Formal analysis and investigation: Guangzheng Dai, Sile Yu; Algorithm development: Shenming Hu, Xinze Luan, Xiaoting Wang, Xinying Liu; Data collection and organization: Hairu Yan, Pengfei Song; Writing—original draft preparation: Guangzheng

Dai; Review and editing: Guangzheng Dai, Sile Yu and Xingru He; Supervision: Xingru He and Sile Yu.

Funding. This study was entirely funded by He University, Shenyang, China. No support was received for the publication of this article. The journal's Rapid Service Fee was funded by the authors.

Data Availability. Anonymized datasets generated and analyzed during the current study will be made available on reasonable request by the corresponding author (Xingru He, hexingru@huh.edu.cn).

Declarations

Conflict of Interest. Xingru He, Guangzheng Dai, Sile Yu, Shenming Hu, Xinze Luan, Hairu Yan, Xiaoting Wang, Pengfei Song and Xinying Liu have nothing to disclose.

Ethical Approval. The study was conducted in compliance with the tenets of the Declaration of Helsinki and the Institutional Review Board of the He Eye Specialist Hospital, Shenyang, China (IRB2019. K010.01). Documented informed consent was obtained from all participants in this study. In the present study, all components with any individually identifiable information have been removed in the dataset.

Open Access. This article is licensed under a Creative Commons Attribution-NonCommercial 4.0 International License, which permits any non-commercial use, sharing, adaptation, distribution and reproduction in any medium or format, as long as you give appropriate credit to the original author(s) and the source, provide a link to the Creative Commons licence, and indicate if changes were made. The images or other third party material in this article are included in the article's Creative Commons licence, unless indicated otherwise in a credit line to the material. If material is not included in the article's Creative Commons licence and your intended use is not permitted by statutory regulation or exceeds the permitted use, you will need to obtain

permission directly from the copyright holder. To view a copy of this licence, visit <http://creativecommons.org/licenses/by-nc/4.0/>.

REFERENCES

- WHO. The top 10 causes of death. WHO; 2020.
- Young A, Garcia M, Sullivan SM, Liu C, Moazzami K, Ko YA, et al. Impaired peripheral microvascular function and risk of major adverse cardiovascular events in patients with coronary artery disease. *Arterioscler Thromb Vasc Biol.* 2021;41(5):1801–9.
- Padro T, Manfrini O, Bugiardini R, Canty J, Cenko E, De Luca G, et al. ESC Working Group on Coronary Pathophysiology and Microcirculation position paper on “coronary microvascular dysfunction in cardiovascular disease.” *Cardiovasc Res.* 2020;116(4):741–55.
- Rocco E, Grimaldi MC, Maino A, Cappannoli L, Pedicino D, Liuzzo G, et al. Advances and challenges in biomarkers use for coronary microvascular dysfunction: from bench to clinical practice. *J Clin Med.* 2022;11(7):2055.
- Sorop O, Olver TD, van de Wouw J, Heinonen I, van Duin RW, Duncker DJ, et al. The microcirculation: a key player in obesity-associated cardiovascular disease. *Cardiovasc Res.* 2017;113(9):1035–45.
- Houben A, Martens RJH, Stehouwer CDA. Assessing microvascular function in humans from a chronic disease perspective. *J Am Soc Nephrol.* 2017;28(12):3461–72.
- Couper DJ, Klein R, Hubbard LD, Wong TY, Sorlie PD, Cooper LS, et al. Reliability of retinal photography in the assessment of retinal microvascular characteristics: the Atherosclerosis Risk in Communities Study. *Am J Ophthalmol.* 2002;133(1):78–88.
- De Boever P, Louwies T, Provost E, Int Panis L, Nawrot TS. Fundus photography as a convenient tool to study microvascular responses to cardiovascular disease risk factors in epidemiological studies. *J Vis Exp.* 2014;92: e51904.
- Panwar N, Huang P, Lee J, Keane PA, Chuan TS, Richhariya A, et al. Fundus photography in the 21st century—a review of recent technological advances and their implications for worldwide healthcare. *Telemed J E Health.* 2016;22(3):198–208.
- Guo S, Yin S, Tse G, Li G, Su L, Liu T. Association between caliber of retinal vessels and cardiovascular disease: a systematic review and meta-analysis. *Curr Atheroscler Rep.* 2020;22(4):16.
- Xue CC, Li C, Hu JF, Wei CC, Wang H, Ahemaitijiang K, et al. Retinal vessel caliber and tortuosity and prediction of 5-year incidence of hypertension. *J Hypertens.* 2023;41(5):830–7.
- Hubbard LD, Brothers RJ, King WN, Clegg LX, Klein R, Cooper LS, et al. Methods for evaluation of retinal microvascular abnormalities associated with hypertension/sclerosis in the Atherosclerosis Risk in Communities Study. *Ophthalmology.* 1999;106(12):2269–80.
- Liew G, Sharrett AR, Kronmal R, Klein R, Wong TY, Mitchell P, et al. Measurement of retinal vascular caliber: issues and alternatives to using the arteriole to venule ratio. *Invest Ophthalmol Vis Sci.* 2007;48(1):52–7.
- Bhuiyan A, Kawasaki R, Lamoureux E, Ramamohanarao K, Wong TY. Retinal artery-vein caliber grading using color fundus imaging. *Comput Methods Progr Biomed.* 2013;111(1):104–14.
- Wong TY, Knudtson MD, Klein R, Klein BE, Meuer SM, Hubbard LD. Computer-assisted measurement of retinal vessel diameters in the Beaver Dam Eye Study: methodology, correlation between eyes, and effect of refractive errors. *Ophthalmology.* 2004;111(6):1183–90.
- Ikram MK, Ong YT, Cheung CY, Wong TY. Retinal vascular caliber measurements: clinical significance, current knowledge and future perspectives. *Ophthalmologica.* 2013;229(3):125–36.
- Liew G, Wang JJ, Cheung N, Zhang YP, Hsu W, Lee ML, et al. The retinal vasculature as a fractal: methodology, reliability, and relationship to blood pressure. *Ophthalmology.* 2008;115(11):1951–6.
- Macgillivray TJ, Patton N, Doubal FN, Graham C, Wardlaw JM. Fractal analysis of the retinal vascular network in fundus images. *Annu Int Conf IEEE Eng Med Biol Soc.* 2007;2007:6456–9.
- Wainwright A, Liew G, Burlutsky G, Rochtchina E, Zhang YP, Hsu W, et al. Effect of image quality, color, and format on the measurement of retinal vascular fractal dimension. *Invest Ophthalmol Vis Sci.* 2010;51(11):5525–9.
- Cosatto VF, Liew G, Rochtchina E, Wainwright A, Zhang Y, Hsu W, et al. Retinal vascular fractal dimension measurement and its influence from imaging variation: results of two segmentation methods. *Curr Eye Res.* 2010;35(9):850–6.
- Cheung CY, Zheng Y, Hsu W, Lee ML, Lau QP, Mitchell P, et al. Retinal vascular tortuosity, blood

- pressure, and cardiovascular risk factors. *Ophthalmology*. 2011;118(5):812–8.
22. Grisan E, Foracchia M, Ruggeri A. A novel method for the automatic grading of retinal vessel tortuosity. *IEEE Trans Med Imaging*. 2008;27(3):310–9.
 23. Bhuiyan A, Nath B, Ramamohanarao K, Kawasaki R, Wong TY. Automated analysis of retinal vascular tortuosity on color retinal images. *J Med Syst*. 2012;36(2):689–97.
 24. Sasongko MB, Wang JJ, Donaghue KC, Cheung N, Benitez-Aguirre P, Jenkins A, et al. Alterations in retinal microvascular geometry in young type 1 diabetes. *Diabetes Care*. 2010;33(6):1331–6.
 25. Cheung CY, Tay WT, Mitchell P, Wang JJ, Hsu W, Lee ML, et al. Quantitative and qualitative retinal microvascular characteristics and blood pressure. *J Hypertens*. 2011;29(7):1380–91.
 26. Li LJ, Kramer M, Tapp RJ, Man RE, Lek N, Cai S, et al. Gestational diabetes mellitus and retinal microvasculature. *BMC Ophthalmol*. 2017;17(1):4.
 27. Li LJ, Lamoureux E, Wong TY, Lek N. Short-term poor glycemic control and retinal microvascular changes in pediatric Type 1 Diabetes patients in Singapore: a pilot study. *BMC Ophthalmol*. 2017;17(1):60.
 28. Ong YT, De Silva DA, Cheung CY, Chang HM, Chen CP, Wong MC, et al. Microvascular structure and network in the retina of patients with ischemic stroke. *Stroke*. 2013;44(8):2121–7.
 29. Patton N, Pattie A, MacGillivray T, Aslam T, Dhillon B, Gow A, et al. The association between retinal vascular network geometry and cognitive ability in an elderly population. *Invest Ophthalmol Vis Sci*. 2007;48(5):1995–2000.
 30. Wang SB, Mitchell P, Liew G, Wong TY, Phan K, Thiagalingam A, et al. A spectrum of retinal vasculature measures and coronary artery disease. *Atherosclerosis*. 2018;268:215–24.
 31. Chapman N, Dell'omo G, Sartini MS, Witt N, Hughes A, Thom S, et al. Peripheral vascular disease is associated with abnormal arteriolar diameter relationships at bifurcations in the human retina. *Clin Sci (Lond, Engl: 1979)*. 2002;103(2):111–6.
 32. Murray CD. The physiological principle of minimum work: II. Oxygen exchange in capillaries. *Proc Natl Acad Sci USA*. 1926;12(5):299–304.
 33. Murray CD. The physiological principle of minimum work: I. The vascular system and the cost of blood volume. *Proc Natl Acad Sci USA*. 1926;12(3):207–14.
 34. Murray CD. The physiological principle of minimum work applied to the angle of branching of arteries. *J Gen Physiol*. 1926;9(6):835–41.
 35. Li L, Verma M, Nakashima Y, Kawasaki R, Nagahara H. Joint learning of vessel segmentation and artery/vein classification with post-processing. *Medical Imaging with deep learning*. PMLR; 2020.
 36. Zamir M, Medeiros JA, Cunningham TK. Arterial bifurcations in the human retina. *J Gen Physiol*. 1979;74(4):537–48.
 37. Zamir M. Nonsymmetrical bifurcations in arterial branching. *J Gen Physiol*. 1978;72(6):837–45.
 38. Dąbrowska EE, Harazny JM, Wolf J, Szulc U, Narkiewicz KJAH. The eye—a window to cardiovascular diseases. *Arter Hypertens*. 2020;24(2):56–60.
 39. Zekavat SM, Raghu VK, Trinder M, Ye Y, Koyama S, Honigberg MC, et al. Deep learning of the retina enables phenome- and genome-wide analyses of the microvasculature. *Circulation*. 2022;145(2):134–50.
 40. Wu R, Cheung CY, Saw SM, Mitchell P, Aung T, Wong TY. Retinal vascular geometry and glaucoma: the Singapore Malay Eye Study. *Ophthalmology*. 2013;120(1):77–83.
 41. Cheung CY, Sabanayagam C, Law AK, Kumari N, Ting DS, Tan G, et al. Retinal vascular geometry and 6-year incidence and progression of diabetic retinopathy. *Diabetologia*. 2017;60(9):1770–81.
 42. Benitez-Aguirre PZ, Sasongko MB, Craig ME, Jenkins AJ, Cusumano J, Cheung N, et al. Retinal vascular geometry predicts incident renal dysfunction in young people with type 1 diabetes. *Diabetes Care*. 2012;35(3):599–604.
 43. Liang C, Gu C, Wang N. Retinal vascular caliber in coronary heart disease and its risk factors. *Ophthalmic Res*. 2022. <https://doi.org/10.1159/000526753>.
 44. Sun C, Liew G, Wang JJ, Mitchell P, Saw SM, Aung T, et al. Retinal vascular caliber, blood pressure, and cardiovascular risk factors in an Asian population: the Singapore Malay Eye Study. *Invest Ophthalmol Vis Sci*. 2008;49(5):1784–90.